Inorganic Chemistry

Article

pubs.acs.org/IC

Lanthanide Coordination Polymers with Tetrafluoroterephthalate as a Bridging Ligand: Thermal and Optical Properties

Christiane Seidel,[†] Chantal Lorbeer,[‡] Joanna Cybińska,[‡,#] Anja-Verena Mudring,[‡] and Uwe Ruschewitz*[,†]

[†]Department of Chemistry, University of Cologne, Greinstraße 6, D-50939 Cologne, Germany

[‡]Anorganische Chemie I – Festkörperchemie und Materialien, Ruhr-Universität Bochum, D-44801 Bochum, Germany

Supporting Information

ABSTRACT: By slow diffusion of triethylamine into a solution of 2,3,5,6-tetrafluoroterephthalic acid (H_2tfBDC) and the respective lanthanide salt in EtOH/DMF single crystals of seven nonporous coordination polymers, $^2_\infty$[Ln(tfBDC)(NO_3)($DMF)_2$]·DMF (Ln^{3+} = Ce, Pr, Nd, Sm, Dy, Er, Yb; *C*2/*c*, *Z* = 8) have been obtained. In the crystal structures, two-dimensional square grids are found, which are composed of binuclear lanthanide nodes connected by $tfBDC^{2-}$ as a linking ligand. The coordination sphere of each lanthanide cation is completed by a nitrate anion and two DMF molecules (CN = 9). This crystal structure is unprecedented in the crystal chemistry of coordination polymers based on nonfluorinated terephthalate (BDC^{2-}) as a bridging ligand; as for $tfBDC^{2-}$, a nonplanar conformation of the ligand is energetically more favorable, whereas for BDC^{2-}, a planar conformation is preferred. Differential thermal analysis/thermogravimetric analysis (DTA/TGA) investigations reveal that the noncoordinating DMF molecule is released first at temperatures of 100–200 °C. Subsequent endothermal weight losses correspond to the release of the coordinating DMF molecules. Between 350 and 400 °C, a strong exothermal weight loss is found, which is probably due to a decomposition of the $tfBDC^{2-}$ ligand. The residues could not be identified. The emission spectra of the $^2_\infty$[Ln(tfBDC)(NO_3)($DMF)_2$]·DMF compounds reveal intense emission in the visible region of light for Pr, Sm, and Dy with colors from orange, orange-red, to warm white.

INTRODUCTION

The interest in coordination polymers, especially in their porous congeners, which are frequently termed MOFs (Metal-Organic Frameworks),[1] has grown rapidly over the past 15 years. Especially, their easy synthetic accessibility and potential applications (e.g., gas storage) have led to numerous publications.[2−10] To improve these properties, MOFs with fluorinated linker molecules came into the focus of discussion and are receiving increasing attention.[11−15] The dianion of terephthalic acid (H_2BDC) is a linker, which is often used for the construction of MOFs (for example, MOF-5[1] or MIL-53[16]). For a perfluorinated counterpart of MOF-5 with the dianion of 2,3,5,6-tetrafluoroterephthalic acid (H_2tfBDC) as a linking ligand, superior H_2 adsorption properties have been predicted by theoretical investigations.[17] On the other hand, a different computational study states that the interaction between H_2 and the fluorinated parts of the framework structure should be even weaker, compared to their nonfluorinated analogues.[18] First experimental results concerning the storage properties of fluorinated MOFs support the assumption of improved storage abilities: a MOF based on triazolate with CF_3 substituents exhibits excellent gas storage capacities for O_2 and H_2.[11] However, to date, there are no reports of a fluorinated counterpart of MOF-5 or any other well-known MOF to compare an isostructural fluorinated and a nonfluorinated substance concerning their storage properties.

Next to storage abilities, coordination polymers are also known to exhibit interesting magnetic and optical properties.[3] Especially in combination with lanthanides, which are known to show strong luminescence, they are supposed to be promising optical materials. First investigations comparing luminescence properties of substances containing Er^{3+} and BDC^{2-}, as well as $tfBDC^{2-}$ as linker ligands, have been presented by Lobkovsky et al.[19] Although the examined compounds $Er_2(BDC)_3(DMF)_2$-$(H_2O)_2$·H_2O and $Er_2(tfBDC)_3(DMF)(H_2O)$·DMF, as well as desolvated $Er_2(BDC)_3$ and partially desolvated $Er_2(tfBDC)_3$-(DMF)·DMF, are not isostructural, important trends were observed. Since solvents such as H_2O and DMF are known to quench luminescence, because of their O–H and C–H vibrations, the desolvated compounds show improved luminescence properties. The modification of the aryl moiety, by means of fluorination, even supports this effect.[19]

Recently, we have been able to improve the well-known synthesis[20] of tetrafluoroterephthalic acid, with respect to yield, resulting in a simplified and less time-consuming purification procedure.[21] With larger quantities of this linker in hand, we were able to synthesize several nonporous coordination polymers with transition metals as well as thallium and lead.[22] Inspired by the results of Lobkovsky et al.,[19] we have now set our focus on the synthesis and characterization of lanthanide-containing tetrafluoroterephthalates. Similar approaches have already been published by other authors.[23,24] After first presenting the results at a conference,[25] we will now give more details of the synthesis and structural properties of these tetrafluoroterephthalates and we will discuss their thermal and optical behavior.

Received: December 9, 2011
Published: March 23, 2012

   dx.doi.org/10.1021/ic202655d | *Inorg. Chem.* 2012, 51, 4679–4688

EXPERIMENTAL SECTION

General Remarks. Tetrafluoroterephthalic acid (H_2tfBDC) was prepared according to the procedure described in the literature.[21] $Dy(NO_3)_3{\cdot}6H_2O$, $Er(NO_3)_3{\cdot}5H_2O$, $Sm(NO_3)_3{\cdot}6H_2O$, $Yb(NO_3)_3{\cdot}5H_2O$ (all from ABCR), $Nd(NO_3)_3{\cdot}6H_2O$ (Alfa Aesar), $Ce(NO_3)_3{\cdot}6H_2O$ (Prolabo), $Pr(NO_3)_3{\cdot}6H_2O$ (Sigma–Aldrich), *N*,*N*′-dimethylformamide (KMF Laborchemie Handels GmbH), and ethanol (Biesterfeld) were used as purchased, without any further purification. Triethylamine (Acros Organics) was distilled prior to the experiment. In all syntheses, yields were not optimized and, therefore, are not given.

Syntheses. $^2_\infty$*[Ce(tfBDC)(NO$_3$)(DMF)$_2$]·DMF (**1**).* 653.5 mg (1.5 mmol, 1.4 equiv) $Ce(NO_3)_3{\cdot}6H_2O$ and 264.3 mg (1.1 mmol, 1.0 equiv) H_2tfBDC were dissolved in 10 mL of a solvent mixture of ethanol and *N*,*N*′-dimethylformamide (3:1, v:v). The snap-cap tube was closed with a cap and the latter was perforated once. It was placed in an exsiccator, whose bottom was filled with 100 mL of the solvent mixture mentioned above. In addition, a beaker with 20 mL of triethylamine dissolved in 20 mL of the same solvent mixture was placed in the exsiccator. After approximately one month, colorless crystals of **1** several millimeters in size were obtained. Elemental analysis for $CeC_{17}H_{21}O_{10}F_4N_4$ (657.50): Calcd — C, 31.06%, H, 3.22%, N, 8.52%; Found — C, 29.30%, H, 3.52%, N, 6.84%. Purity was additionally checked by X-ray powder diffraction (XRPD) (see Figure S1 in the Supporting Information). Both investigations indicate that no single-phase sample was obtained. Therefore, only the results of the X-ray single-crystal structure analysis of **1** are given in the following. For IR data (KBr), see Figure S12 in the Supporting Information.

$^2_\infty$*[Pr(tfBDC)(NO$_3$)(DMF)$_2$]·DMF (**2**).* A similar procedure using 652.6 mg (1.5 mmol, 1.4 equiv) $Pr(NO_3)_3{\cdot}6H_2O$ and 264.2 mg (1.1 mmol, 1.0 equiv) H_2tfBDC yielded green crystals of **2**. Elemental analysis for $PrC_{17}H_{21}O_{10}F_4N_4$ (658.29): Calcd — C, 31.02%, H, 3.22%, N, 8.51%; Found — C, 30.50%, H, 3.39%, N, 8.37%. Purity was additionally checked by XRPD (see Figure S2 in the Supporting Information) indicating a single phase sample. IR (KBr, cm^{-1}): 3431 (b), 3024 (w), 2970 (w), 2947 (m), 2854 (w), 2814 (w), 2752 (w), 2582 (w), 2499 (w), 2378 (w), 2314 (w), 2112 (w), 2060 (w), 2029 (w), 1996 (w), 1983 (w), 1952 (w), 1676 (s), 1639 (s), 1583 (m), 1498 (m), 1477 (s), 1468 (w), 1435 (m), 1402 (s), 1383 (s), 1294 (s), 1252 (m), 1153 (w), 1115 (m), 1092 (m), 1061 (m), 1032 (m), 989 (s), 918 (w), 866 (w), 816 (w), 781 (w), 752 (s), 727 (s), 675 (s), 660 (m), 629 (w), 476 (m), 417 (w) (see Figure S12 in the Supporting Information).

$^2_\infty$*[Nd(tfBDC)(NO$_3$)(DMF)$_2$]·DMF (**3**).* A similar procedure using 660.4 mg (1.5 mmol, 1.4 equiv) $Nd(NO_3)_3{\cdot}6H_2O$ and 263.1 mg (1.1 mmol, 1.0 equiv) H_2tfBDC yielded purple crystals of **3**. Elemental analysis for $NdC_{17}H_{21}O_{10}F_4N_4$ (661.62): Calcd — C, 30.86%, H, 3.20%, N, 8.47%; Found — C, 30.31%, H, 3.16%, N, 9.07%. Purity was additionally checked via XRPD (see Figure S3 in the Supporting Information), indicating a single-phase sample. IR (KBr, cm^{-1}): 3425 (b), 3024 (w), 2968 (w), 2947 (m), 2854 (w), 2816 (w), 2754 (w), 2603 (w), 2499 (w), 2378 (w), 2316 (w), 2112 (w), 2060 (w), 2029 (w), 1998 (w), 1984 (w), 1952 (w), 1676 (s), 1637 (s), 1583 (m), 1500 (m), 1477 (s), 1466 (w), 1437 (m), 1404 (s), 1385 (s), 1294 (s), 1254 (m), 1153 (w), 1115 (m), 1092 (m), 1061 (m), 1032 (m), 989 (s), 918 (w), 866 (w), 816 (w), 781 (w), 752 (s), 727 (s), 677 (s), 660 (m), 631 (w), 478 (m), 417 (w) (see Figure S12 in the Supporting Information).

$^2_\infty$*[Sm(tfBDC)(NO$_3$)(DMF)$_2$] · DMF (**4**).* A similar procedure using 670.5 mg (1.5 mmol, 1.4 equiv) $Sm(NO_3)_3{\cdot}6H_2O$ and 263.0 mg (1.1 mmol, 1.0 equiv) H_2tfBDC yielded yellow crystals of **4**. Elemental analysis for $SmC_{17}H_{21}O_{10}F_4N_4$ (667.73): Calcd — C, 30.58%, H, 3.17%, N, 8.39%; Found — C, 29.76%, H, 3.22%, N, 8.19%. Purity was additionally checked by XRPD (see Figure S4 in the Supporting Information), indicating a single-phase sample. IR (KBr, cm^{-1}): 3429 (b), 3024 (w), 2968 (w), 2947 (m), 2854 (w), 2816 (w), 2754 (w), 2586 (w), 2501 (w), 2378 (w), 2320 (w), 2112 (w), 2062 (w), 2031 (w), 2000 (w), 1984 (w), 1952 (w), 1676 (s), 1637 (s), 1583 (m), 1500 (m), 1477 (s), 1466 (w), 1437 (m), 1406 (s), 1385 (s), 1298 (s), 1254 (m), 1153 (w), 1117 (m), 1092 (m), 1061 (m), 1034 (m), 989 (s), 920 (w), 868 (w), 816 (w), 783 (w), 754 (s), 727 (s), 677 (s), 660 (m), 631 (w), 478 (m), 417 (w) (see Figure S12 in the Supporting Information).

$^2_\infty$*[Dy(tfBDC)(NO$_3$)(DMF)$_2$]·DMF (**5**).* A similar procedure using 685.2 mg (1.5 mmol, 1.4 equiv) $Dy(NO_3)_3{\cdot}6H_2O$ and 264.3 mg (1.1 mmol, 1.0 equiv) H_2tfBDC yielded colorless crystals of **5**. Elemental analysis for $DyC_{17}H_{21}O_{10}F_4N_4$ (679.88): Calcd — C, 30.03%, H, 3.11%, N, 8.24%; Found — C, 29.67%, H, 3.23%, N, 9.01%. Purity was additionally checked by XRPD (see Figure S5 in the Supporting Information), indicating a single-phase sample. IR (KBr, cm^{-1}): 3433 (b), 3024 (w), 2980 (w), 2949 (m), 2854 (w), 2816 (w), 2754 (w), 2600 (w), 2507 (w), 2379 (w), 2328 (w), 2114 (w), 2067 (w), 2031 (w), 2006 (w), 1984 (w), 1952 (w), 1676 (s), 1639 (s), 1585 (m), 1500 (m), 1479 (s), 1466 (w), 1434 (m), 1410 (s), 1385 (s), 1304 (s), 1252 (m), 1155 (w), 1117 (m), 1092 (m), 1063 (m), 1036 (m), 989 (s), 922 (w), 868 (w), 816 (w), 783 (w), 756 (s), 723 (s), 687 (s), 660 (m), 631 (w), 482 (m), 417 (w) (see Figure S12 in the Supporting Information).

$^2_\infty$*[Er(tfBDC)(NO$_3$)(DMF)$_2$]·DMF (**6**).* A similar procedure using 666.6 mg (1.5 mmol, 1.4 equiv) $Er(NO_3)_3{\cdot}5H_2O$ and 262.4 mg (1.1 eq., 1.0 equiv) H_2tfBDC yielded pink crystals of **6**. Elemental analysis for $ErC_{17}H_{21}O_{10}F_4N_4$ (684.64): Calcd — C, 29.82%, H, 3.09%, N, 8.18%; Found — C, 29.75%, H, 3.31%, N, 8.60%. Purity was additionally checked by XRPD (see Figure S6 in the Supporting Information), indicating a single-phase sample. IR (KBr, cm^{-1}): 3430 (b), 3023 (w), 2980 (w), 2945 (m), 2856 (w), 2816 (w), 2754 (w), 2603 (w), 2509 (w), 2380 (w), 2332 (w), 2114 (w), 2069 (w), 2031 (w), 2010 (w), 1984 (w), 1954 (w), 1676 (s), 1639 (s), 1585 (m), 1500 (m), 1479 (s), 1466 (w), 1435 (m), 1414 (s), 1385 (s), 1306 (s), 1254 (m), 1153 (w), 1117 (m), 1092 (m), 1063 (m), 1038 (m), 989 (s), 924 (w), 870 (w), 816 (w), 785 (w), 756 (s), 729 (s), 687 (s), 660 (m), 631 (w), 482 (m), 418 (w) (see Figure S12 in the Supporting Information).

$^2_\infty$*[Yb(tfBDC)(NO$_3$)(DMF)$_2$]·DMF (**7**).* A similar procedure using 675.6 mg (1.5 mmol, 1.4 equiv) $Yb(NO_3)_3{\cdot}5H_2O$ and 264.3 mg (1.1 mmol, 1.0 equiv) H_2tfBDC yielded colorless crystals of **7**. Elemental analysis for $YbC_{17}H_{21}O_{10}F_4N_4$ (690.42): Calcd — C, 29.57%, H, 3.07%, N, 8.12%; Found — C, 27.60%, H, 2.59%, N, 10.42%. Purity was additionally checked by XRPD (see Figure S7 in the Supporting Information). Both investigations indicate that no single-phase sample was obtained. Therefore, only the results of the X-ray single-crystal structure analysis of **7** are given in the following. For IR data (KBr), see Figure S12 in the Supporting Information.

X-ray Single Crystal Structure Analysis. Single crystals of **1**–**7** were isolated and mounted in sealed glass capillaries on a Stoe IPDS I, IPDS II or Nonius Kappa CCD ($T \approx 293$ K, Mo Kα radiation). The latter was chosen for a low-temperature analysis of compound **4** at 100 K. For data collection and reduction of crystals measured on the Stoe diffractometers, the Stoe program package[26] was applied. Data collected on the Nonius Kappa CCD were treated with COLLECT[27] for data collection and DENZO[28] for data reduction. The structural models were solved using SIR-92[29] and completed using difference Fourier maps calculated with SHELXL-97,[30] which was also used for final refinements. These programs were run under the WinGX system.[31] All non-hydrogen atoms were refined anisotropically. Hydrogen atoms of DMF molecules were calculated and refined "riding" with fixed distances (93 pm (C(O)H group), 96 pm (CH_3 group)). Details of all single-crystal structure analyses are given in Table 1.[32]

X-ray Powder Diffraction. XRPD data were collected at room temperature on a Huber Model G670 system with a germanium monochromator, using Cu Kα_1 radiation and an imaging plate detector. To compensate for the strong absorption of lanthanide-containing compounds, the measurements were carried out as flat samples with the substances placed between two foils (reflections due to the foil: 2θ = 21.5° and 23.7°). Exposure time was 60 min. Employing the WinXPow software suite,[33] the recorded patterns were compared with theoretical patterns calculated from single-crystal structure data.

dx.doi.org/10.1021/ic202655d | Inorg. Chem. 2012, 51, 4679–4688

Table 1. Details of X-ray Single-Crystal Structure Analysis of Compounds 1−7

	1	2	3	4	4a	5	6	7
formula	$CeC_{17}H_{21}F_4N_4O_{10}$	$PrC_{17}H_{21}F_4N_4O_{10}$	$NdC_{17}H_{21}F_4N_4O_{10}$	$SmC_{17}H_{21}F_4N_4O_{10}$	$SmC_{17}H_{21}F_4N_4O_{10}$	$DyC_{17}H_{21}F_4N_4O_{10}$	$ErC_{17}H_{21}F_4N_4O_{10}$	$YbC_{17}H_{21}F_4N_4O_{10}$
formula weight [g mol^{-1}]	657.50	658.29	661.62	667.73	667.73	679.88	684.64	690.42
crystal description	blocks, colorless	blocks, green	blocks, violet	blocks, yellow	blocks, yellow	blocks, colorless	blocks, pink	blocks, colorless
crystal size [mm]	0.18 × 0.15 × 0.13	0.20 × 0.20 × 0.10	0.31 × 0.27 × 0.21	0.30 × 0.30 × 0.20	0.40 × 0.20 × 0.10	0.20 × 0.15 × 0.10	0.67 × 0.26 × 0.21	0.34 × 0.18 × 0.17
space group	$C2/c$ (No. 15)	$C2/c$ (No. 15)	$C2/c$ (No. 15)	$C2/c$ (No. 15)	$C2/c$ (No. 15)	$C2/c$ (No. 15)	$C2/c$ (No. 15)	$C2/c$ (No. 15)
Z	8	8	8	8	8	8	8	8
a [pm]	2222.7(4)	2216.98(7)	2217.0(3)	2210.79(9)	2183.6(1)	2204.2(1)	2199.4(3)	2199.0(4)
b [pm]	1153.4(2)	1149.36(4)	1147.9(1)	1142.66(4)	1140.02(7)	1134.38(5)	1128.50(9)	1125.7(2)
c [pm]	2072.8(3)	2067.86(7)	2066.3(3)	2060.25(8)	2042.84(8)	2054.7(1)	2048.0(3)	2050.6(4)
β [deg]	110.98(1)	111.053(2)	111.11(2)	111.223(2)	111.456(3)	111.466(2)	111.44(2)	111.47(2)
V [× 10^6 pm^3]	4962(1)	4917.4(3)	4906(1)	4851.6(3)	4733.0(4)	4781.2(4)	4732(1)	4724(1)
calc. density [g cm^{-3}]	1.760	1.778	1.792	1.828	1.874	1.889	1.922	1.941
absorption correction	numerical	numerical	numerical	numerical	numerical	numerical	numerical	numerical
diffractometer, radiation	IPDS II, Mo Kα	Nonius Kappa CCD, Mo Kα	IPDS I, Mo Kα	Nonius Kappa CCD, Mo Kα	Nonius Kappa CCD, Mo Kα	Nonius Kappa CCD, Mo Kα	IPDS I, Mo Kα	IPDS I, Mo Kα
temperature [K]	293(2)	293(2)	293(2)	293(2)	100(2)	293(2)	293(2)	293(2)
$2\theta_{max}$ [deg]	54.78	54.94	56.3	54.94	54.96	54.86	56.3	56.3
index ranges	$-28 \le h \le 28$ $-14 \le k \le 13$ $-26 \le l \le 26$	$-28 \le h \le 28$ $-14 \le k \le 13$ $-26 \le l \le 27$	$-29 \le h \le 29$ $-15 \le k \le 15$ $-24 \le l \le 25$	$-28 \le h \le 27$ $-14 \le k \le 14$ $-26 \le l \le 26$	$-28 \le h \le 17$ $-13 \le k \le 14$ $-26 \le l \le 22$	$-28 \le h \le 19$ $-10 \le k \le 14$ $-18 \le l \le 26$	$-28 \le h \le 29$ $-14 \le k \le 14$ $-26 \le l \le 26$	$-29 \le h \le 28$ $-13 \le k \le 13$ $-27 \le l \le 27$
reflections collected/independent	38422/5577	19357/5630	22764/5613	22833/5568	11194/5370	14621/5391	21856/5699	27768/5403
significant reflections	3093 with I > 2σ(F^2)	4609 with I > 2σ(F^2)	4051 with I > 2σ(F^2)	4465 with I > 2σ(F^2)	4419 with I > 2σ(F^2)	4497 with I > 2σ(F^2)	4912 with I > 2σ(F^2)	4094 with I > 2σ(F^2)
R(int)	0.1607	0.0405	0.0790	0.0753	0.0532	0.0397	0.0278	0.0507
data/parameters/restraints	5577/336/0	5630/336/0	5613/335/0	5568/336/0	5370/336/0	5391/336/0	5699/336/0	5403/335/0
GooF = S_{all}	0.917	1.066	0.914	1.109	1.005	1.028	1.143	1.017
R [$F^2 > 2\sigma(F^2)$]	0.0572	0.0253	0.0369	0.0423	0.0288	0.0240	0.0242	0.0260
$wR(F^2)$	0.1597	0.0613	0.0913	0.1093	0.0697	0.0506	0.0681	0.0539
$\Delta\rho_{max}/\Delta\rho_{min}$ [× 10^{-6} pm^{-3}]	−1.414/1.292	−0.448/0.507	−1.486/1.766	−1.650/2.134	−1.507/1.110	−0.548/0.506	−0.806/0.689	−1.027/1.165

dx.doi.org/10.1021/ic202655d | Inorg. Chem. 2012, 51, 4679−4688

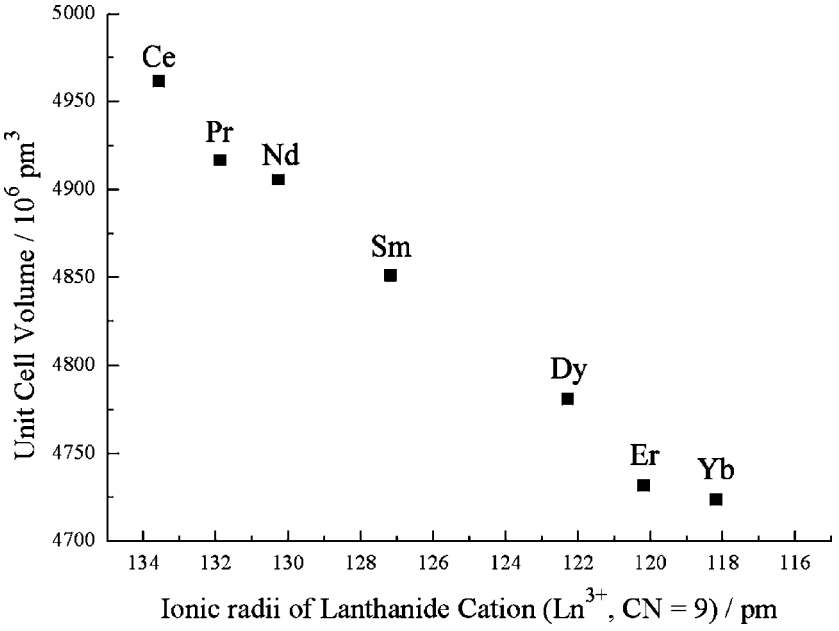

Figure 1. Dependence of unit-cell volume of $^{2}_{\infty}$[Ln(tfBDC)(NO_3)($DMF)_2$]·DMF on the ionic radii of the respective lanthanides.

Table 2. Ionic Radii, Unit Cell Volumes, and Selected Interatomic Distances of Compounds 1−7

				Interatomic Distance [pm]		
Ln^{3+} atom	corresponding compound	ionic radii (CN = 9)[34] [pm]	volume [× 10^6 pm^3]	Ln^{3+}−Ln^{3+}	Ln^{3+}−O1	Ln^{3+}−O6
Ce	**1**	133.6	4962(1)	417.7(1)	246.8(6)	246.7(6)
Pr	**2**	131.9	4917.4(3)	414.88(2)	245.4(2)	245.0(2)
Nd	**3**	130.3	4906(1)	412.31(8)	244.6(3)	244.1(3)
Sm	**4**	127.2	4851.6(3)	408.32(4)	241.1(4)	240.6(4)
Sm	**4a**	127.2	4733.0(4)	408.33(6)	239.8(2)	240.0(2)
Dy	**5**	122.3	4781.2(4)	402.38(3)	236.0(2)	235.8(2)
Er	**6**	120.2	4732(1)	400.26(9)	233.0(2)	233.4(2)
Yb	**7**	118.2	4724(1)	399.9(1)	230.5(3)	230.8(3)

Elemental Analysis. Elemental analyses were carried out with a HEKAtech CHNS Euro EA 3000 system.

Thermoanalytical Investigations. Differential thermal analysis (DTA) and thermogravimetric analysis (TG) were performed for all compounds **2**−**6** in Al_2O_3 containers. The sample masses range from 18.9 mg to 25.0 mg. Temperature intervals are 20−600 °C (**2**, **4**) and 40−600 °C (**3**, **5**, **6**), with heating rates of 15 °C/min. The instrument (Netzsch, Model STA 409C) is housed in a glovebox (M. Braun, Garching/Germany, nitrogen atmosphere) and the sample chamber is continuously flushed with argon at a rate of 70 mL/min.

Infrared Spectroscopy. Infrared (IR) measurements were carried out on KBr pellets using a Bruker IFS 66v/S system with a Nernst globar.

Absorption. Visible and near infrared (NIR) absorption spectra were measured at room temperature on a Cary Model 5000 spectrometer (Varian, Palo Alto, CA). For the measurements, pellets of the solid samples were prepared and fixed in the sample holder.

Luminescence Spectroscopy. Fluorescence measurements were carried out on a Fluorolog FL 3-22 spectrometer (Horiba Jobin Yvon, Unterhachingen, Germany). A continuous xenon lamp with 450 W is used for sample excitation. Double gratings for the excitation and emission are employed as monochromators. The signal is detected by a photomultiplier. For the measurements, crystals were freshly taken from the supernatant solvent mixture, dried with a tissue, ground, and filled in silica tubes, which were carefully positioned in the incoming beam in the sample chamber. For the measurements at low temperatures, the silica tubes were placed in a liquid-nitrogen-filled Dewar equipped with special optical glass windows.

RESULTS AND DISCUSSION

Compounds **1**−**7** crystallize in the monoclinic spacegroup *C*2/*c* (No. 15) with eight formula units per unit cell. For these compounds, the expected trends are found, i.e., decreasing unit cell volumes (Figure 1) and Ln−O distances (see Table 2 and Figure S13 in the Supporting Information), in agreement with the decreasing radii of the respective lanthanide cations (CN = 9).[34] All of the compounds, with the exception of **1** and **7**, crystallizes as pure phases, as the results of elemental analysis and XRPD confirm. Since **1**−**7** are isostructural, only the structure of **2** will be discussed in detail.

The Pr cation sits on a general position and is surrounded by nine O atoms to form a distorted monocapped rectangular antiprism (see Figure 2). Two O atoms belong to a bidentately coordinating nitrate anion (Pr−O21, 255.1(2) pm; Pr−O23, 257.3(2) pm) and two further ones to DMF molecules (Pr−O11, 243.8(2) pm; Pr−O14, 244.6(2) pm). Two carboxylate groups of tetrafluoroterephthalate are chelating two Pr cations bidentately to form a binuclear secondary building unit (SBU) (Pr−O1, 245.4(2) pm; Pr−O6, 245.0(2) pm). The coordination sphere is completed by two tridentately bridging carboxylate groups: two O atoms coordinate in a chelating mode to the same cation (Pr−O7A,: 270.0(2) pm; Pr−O7B, 256.4(2) pm). O7A is also coordinating to the second Pr cation of the binuclear unit (Pr−O7A, 245.6(2) pm). Because of the inversion symmetry of the binuclear unit, the carboxylate group

dx.doi.org/10.1021/ic202655d | *Inorg. Chem.* 2012, 51, 4679−4688

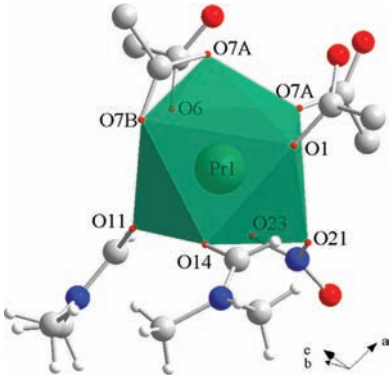

Figure 2. Coordination sphere of Pr^{3+} in $^{2}_{\infty}[Pr(tfBDC)(NO_3)(DMF)_2]\cdot DMF$ (**2**). Coordinating O atoms are reduced in size and $tfBDC^{2-}$ ligands are only partly shown (Pr, green; O, red; C, light gray; N, blue; and H, white).

of the second ligand is completing the coordination sphere of Pr with CN = 9 (Figure 3). The binuclear unit and four

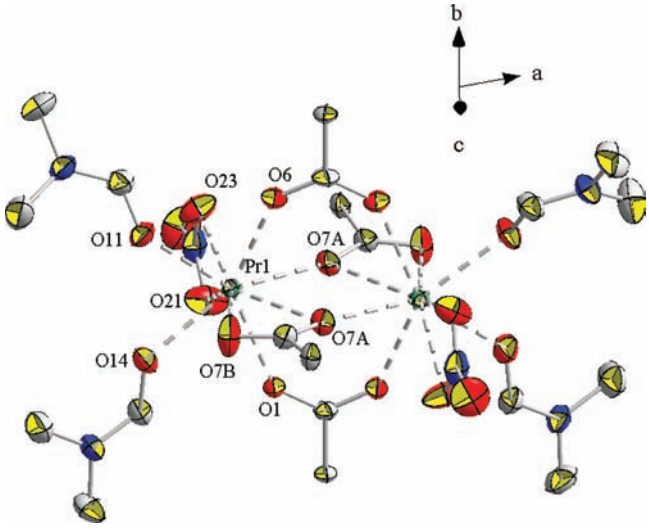

Figure 3. ORTEP diagram of the binuclear unit in $^{2}_{\infty}[Pr(tfBDC)(NO_3)(DMF)_2]\cdot DMF$ (**2**) showing 50% probability thermal ellipsoids and the atomic numbering scheme. H atoms of the DMF molecule have been omitted for clarity, Pr−O connections are drawn as broken lines and $tfBDC^{2-}$ linker molecules are only partly depicted (Pr, green; O, red; C, light gray; and N, blue).

$tfBDC^{2-}$ ligands form distorted paddlewheel-like units, which are connected among each other to two-dimensional layers spreading out in the (100) plane (see Figure 4). Such small windows are generated with a size of ~700−760 pm measuring the distances between the centers of fluorine atoms of opposite ligands. However, since adjacent layers are packed in a staggered way along the [100] axis, no channels are formed. Moreover, a further noncoordinating DMF molecule per formula unit acts as a spacer between the layers. It is located above and below the window described above (see Figure 5).

Recently, a similar crystal structure was described for $^{2}_{\infty}[Ln_2(tfBDC)_3(DEF)_2(EtOH)_2]\cdot 2DEF$ with Ln^{3+} = Tb, Gd, Eu, La, Nd (*C*2/*c*, Z = 4).[23] The Ln cation also forms LnO_9 polyhedra (tricapped trigonal prisms), which are connected to binuclear units. These binuclear units are connected by the $tfBDC^{2-}$ ligands to form sheets (4^4 nets), which stack along the

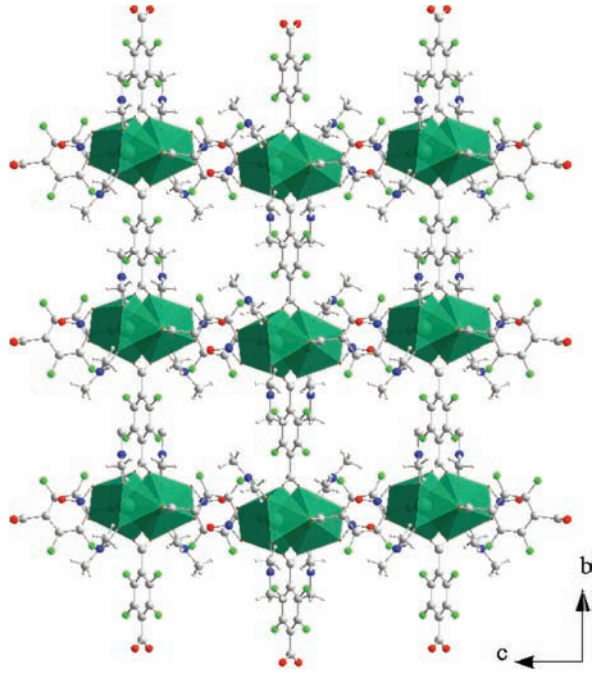

Figure 4. View of the crystal structure of $^{2}_{\infty}[Pr(tfBDC)(NO_3)(DMF)_2]\cdot DMF$ (**2**) along the [100] direction, showing one polymeric layer (4^4 net). Noncoordinating DMF molecules have been omitted for clarity. (Pr, dark green; O, red; C, light gray; N, blue; F, light green; and H, white.

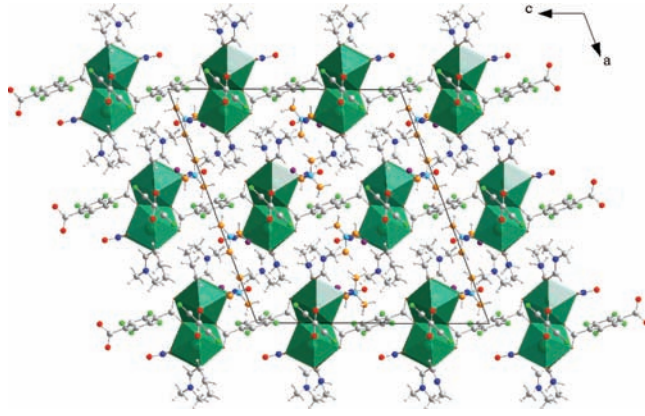

Figure 5. View of the crystal structure of $^{2}_{\infty}[Pr(tfBDC)(NO_3)(DMF)_2]\cdot DMF$ (**2**) along the [010] direction. For coloring of atoms, see Figure 4. Noncoordinating DMF molecules are shown in a different color.

crystallographic *a*-axis. Therefore, the topologies of both crystal structures (ref 23 and this work) are quite similar, but the (formal) replacement of half a $tfBDC^{2-}$ ligand by NO_3^- leads to a different connectivity within the layers. In this work,[23] the luminescence properties of the terbium and europium compounds also were presented. However, since these cations are not part of our work, these measurements will not be discussed in comparison to our own spectroscopic results (see below).

It is a noteworthy and well-known aspect of tetrafluoroterephthalates[35,36] that the carboxylate groups of the linker are twisted out of the plane of the aryl moiety. This is a result of the electrostatic repulsion between the F atoms of the ring and the O atoms of the carboxylate groups. Furthermore, the

dx.doi.org/10.1021/ic202655d | *Inorg. Chem.* 2012, 51, 4679−4688

electron-withdrawing nature of the F atoms reduces the electron density in the aromatic ring considerably and such its aromatic character, which lowers the energy for a twist of the carboxylate groups out of the plane of the aryl moiety significantly.[35,36] According to the literature, one finds torsion angles of >20° in most tetrafluoroterephthalates.[22,35] The coordination polymers presented in this work contain two crystallographically independent linker molecules (see Figure 6).

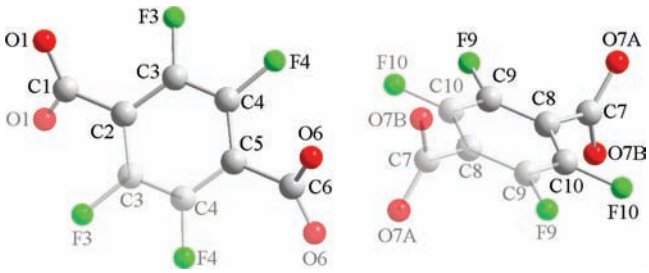

Figure 6. View of the two crystallographically independent linker molecules I (left) and II (right) in $^{2}_{\infty}$[Pr(tfBDC)(NO_3)($DMF)_2$]·DMF (**2**) with atomic numbering scheme. Transparent presentation is chosen for those atoms generated by symmetry operations.

For compounds **1**–**7**, the torsion angle values range from 47.3(2)° to 52.0(2)° (linker I) and from 77.3(4)° to 80.3(8)° (linker II).

To investigate possible structural changes upon cooling, the samarium compound (**4**) was selected for a low-temperature X-ray single-crystal structure analysis. As expected, the thermal ellipsoids and lattice constants decrease, and the unit-cell volume is reduced by ~120 × 10^6 pm^3. As a consequence, the torsion angles of linker II decrease by 6.0° and 4.2°. For linker I, the decrease is less significant (1.3° and 1.4°, respectively). The shortest distance between two Sm atoms of adjacent layers decreases from 966.76(5) pm to 958.11(4) pm as well as the distance within one layer from 1034.05(6) pm to 1027.10(5) pm (see Tables 2 and 3).

Table 3. Torsion Angles of $^{2}_{\infty}$[Sm(tfBDC)(NO_3)($DMF)_2$]·DMF at 293 K (4) and 100 K (4a)

	Torsion Angle [deg]	
	4 (293 K)	**4a** (100 K)
O1—C1—C2—C3	−48.3(4)	−47.0(2)
C4—C5—C6—O6	51.6(4)	50.2(2)
O7B—C7—C8—C10	80.3(8)	74.2(4)
O7A—C7—C8—C9	79.2(7)	75.0(4)

Thermoanalytical investigations were performed on compounds **2**–**6**. As an example, the recorded DTA and TG curves of the Nd compound (**3**) are shown in Figure 7. The curves of all of the other compounds are given in the Supporting Information (Figures S8–S11). The DTA curve of **3** shows two endothermic signals (at 150 and 180 °C), followed by two exothermic signals at 310 and 380 °C. The endothermic events are accompanied by a continuous mass loss of ~18%, followed by a mass loss of 15% for the first exothermic signal. The sum of both (33%) is in perfect agreement with the loss of three DMF molecules, for which 33% is calculated. The second exothermic signal leads to another mass loss of ~20%. This can be interpreted as a decomposition of the ligands. The

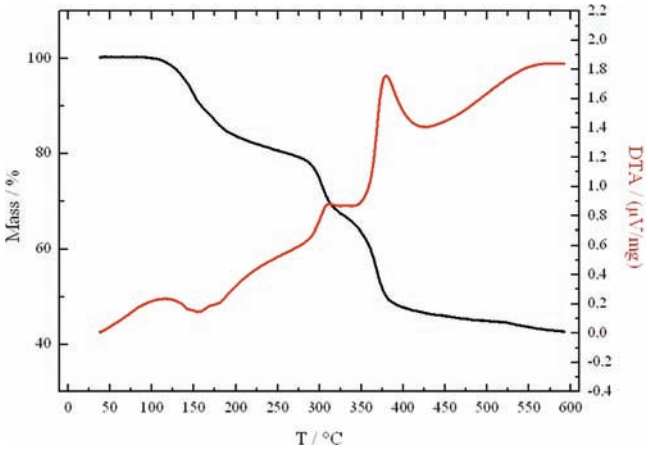

Figure 7. DTA (red) and TG (black) curves of $^{2}_{\infty}$[Nd(tfBDC)(NO_3)-($DMF)_2$]·DMF (**3**).

remaining mass at 500 °C (298 g/mol) is much larger than the value calculated for one-half of a formula unit of Nd_2O_3 (168 g/mol) and NdOF (179 g/mol). LnOF was obtained after heating Ln_2(tfBDC)$_3$($DEF)_2$($EtOH)_2$·2DEF.[23] Similar DTA and TG curves are obtained for **2** (see Table S1 and Figure S8 in the Supporting Information). Here, the mass losses of the first two events are 34%, and the final exothermic events point to a decomposition of the ligands. For **2**, this decomposition proceeds explosively, thus expelling sample from the container (mass remaining at 500 °C: 10%). A different behavior is observed for the compounds **4**–**6** (see Table S1 and Figures S9–S11 in the Supporting Information). Two or three endothermic events, starting at ~150 °C, lead to a mass loss of 20%–22%, in agreement with the release of two DMF molecules. This is followed by 1–2 exothermic events pointing to a decomposition of the ligand and eventually including a release of the remaining DMF molecule. The remaining mass at 500 °C is similar to that of **2** (42%–44%) and, thus, is much higher than the calculated value for Ln_2O_3 or LnOF (27%–29% and 28%–30%). For compound **4**, similar to that observed for **2**, a heavy decomposition is observed, which obviously expels sample from the container (remaining mass at 500 °C: 6%). The results of the thermoanalytical investigations on compounds **2**–**6** are summarized in Table S1 in the Supporting Information. It should be mentioned that the assignment of mass losses can, in most cases, only be approximated, because most thermal events follow each other continuously. This definitely hampers a more detailed analysis of the data we obtained; therefore, our interpretation is still somewhat vague. An analysis of the released gases as well as an elemental analysis and an XRPD investigation of the residues obtained after heating will be part of our future work on these compounds. It was already found that the residue obtained after heating up to 600 °C is of poor crystallinity and could not be assigned to any known lanthanide compound up to now. But preliminary elemental analyses of samples heated to temperatures, where a release of DMF was speculated, confirm our interpretation of the data. In future experiments it will be our goal to obtain solvent-free compounds. The DTA/TG results clearly indicate that compounds **2** and **3** are the most promising candidates for such an approach.

Lanthanide ions are well-known to give rise to luminescence and are used as optical active centers in many of the phosphors used for lighting, scintillating, and plasma display panel applications.[37–41]

dx.doi.org/10.1021/ic202655d | Inorg. Chem. 2012, 51, 4679–4688

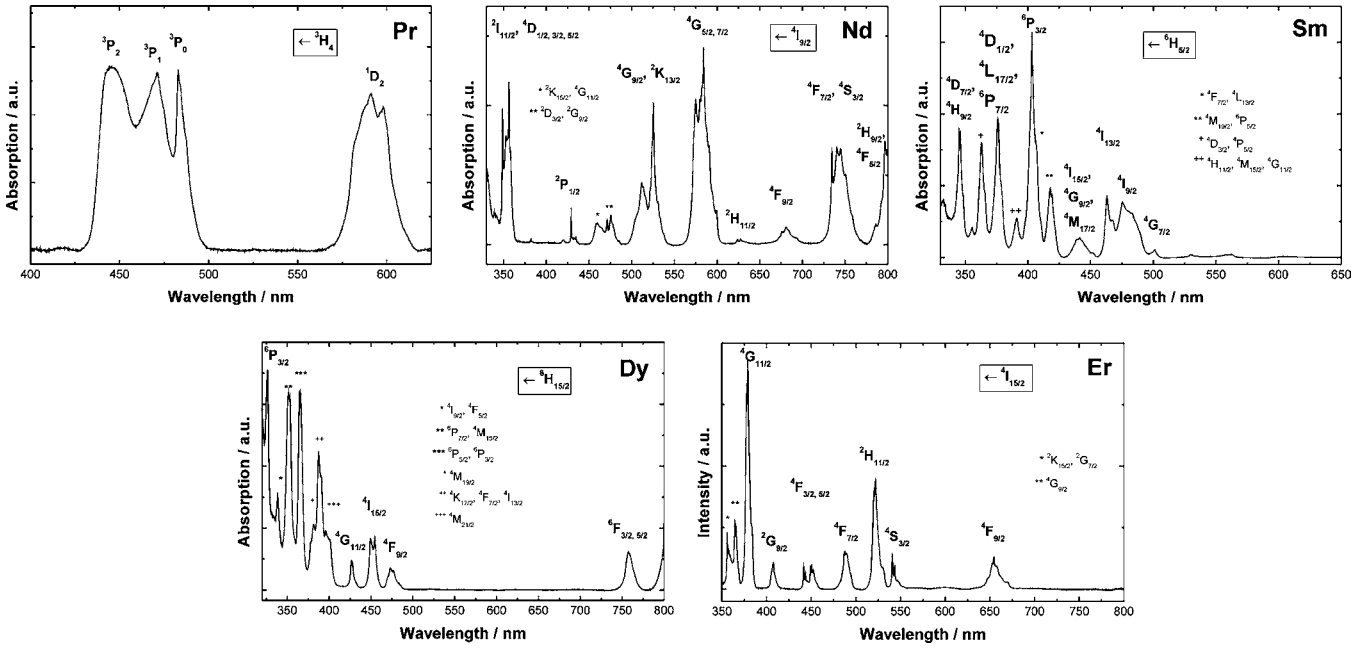

Figure 8. Room-temperature absorption spectra of the $^{2}_{\infty}$[Ln(tfBDC)$(NO_3)(DMF)_2$]·DMF compounds **2**–**6**.

The characteristic luminescence of trivalent lanthanide ions mainly arises from intraconfigurational f–f transitions, which lead to sharp line emission spectra, as a result of the imperfect shielding of the f-electrons. Because of that, the influence of the chemical environment of the Ln^{3+} ion on the location of the energy levels can typically be neglected. However, there are some transitions that are sensitive to the coordination environment of the Ln ion. They obey the selection rules $|\Delta S| = 0$, $|\Delta L| \leq 2$, $|\Delta J| \leq 1$, and are called hypersensitive. Also, the coordination environment of the Ln ion, as well as the total crystal structure, may influence luminescence, since multiphonon relaxation processes can bridge energy gaps between emitting levels and therefore may lead to nonradiative deactivation of excited states.

To study the optical properties of the $^{2}_{\infty}$[Ln(tfBDC)(NO_3)-$(DMF)_2$]·DMF compounds, the absorption spectra were recorded (see Figure 8). The room-temperature absorption spectra entirely consist of the f–f transitions expected for the respective trivalent Ln ions. The color of the crystal is equal to the complementary color of the absorbed color.[42] These colors that arise from intraconfigurational f–f transitions within trivalent lanthanide (Ln^{3+}) ions are well-known. The main absorption of the Pr^{3+} compound (**2**) originates from the $^3H_4$ ground state. The main absorption lines are observed in the violet–blue (440–480 nm, $^3P_J \leftarrow {}^3H_4$) region of light with some smaller orange–red contribution at ~585 nm ($^1D_2 \leftarrow {}^3H_4$). The complementary color is green, which is indeed observed by the naked eye. The Nd^{3+} ion in compound **3** shows a rich level structure with several absorption lines from UV to NIR dominated by the $^4G_{5/2,7/2} \leftarrow {}^4I_{9/2}$ transitions at 525 nm and the $^4G_{9/2}, {}^2K_{13/2} \leftarrow {}^4I_{9/2}$ transitions at 580 nm yielding a purple crystal color. The Sm^{3+} compound **4** exhibits a set of transitions arising from the $^6H_{5/2}$ ground state with energies above 20 000 cm^{-1} (500 nm) and only very weak ones below. This absorption in the blue and violet region explains the yellowish appearance of the material. The same is found for the Dy^{3+} compound (**5**), where only a pale white-yellow color of the crystals is expected, because of the relatively high energy of the absorption lines resulting from the $^6H_{15/2}$ ground state. The Er^{3+} compound (**6**) reveals several absorption lines in the entire visible region resulting from $^4F_J \leftarrow {}^4I_{15/2}$ and $^2G_{9/2}$, $^2H_{11/2}$, $^4S_{3/2} \leftarrow {}^4I_{15/2}$ transitions concluding in a pink color. In summary, the measured absorption spectra and the appearance of the obtained lanthanide compounds are in agreement with results obtained on other lanthanide compounds.[42−44] Since the tetrafluoroterephthalate ligand exhibits no absorption in the visible region of light, the color of the crystals only results from the intrinsic Ln^{3+} transitions, as proven by the absorption spectra.

The Ln ions present in the compounds discussed herein can show emissions in the visible and IR ranges. The visible emissions of the Pr (**2**), Sm (**4**), and Dy (**5**) compounds are displayed in Figure 9. Sm^{3+} and Dy^{3+}, although less-intense emitters, in comparison to Eu^{3+} or Tb^{3+}, currently gain interest with the progress in dual luminescent time-resolved immunoassay techniques.[45] Pr^{3+} is a versatile luminescent center and is well-known for the up-conversion as well as the quantum cutting phenomenon.[46,47]

The luminescence of non-Kramer Pr^{3+} ions with $4f^2$ ground-state configuration can theoretically occur from three emitting levels: $^3P_0$, $^1D_2$, or $^1G_4$. Albeit, depending on the system, solely emission from $^3P_0$ or $^1D_2$ is observed. The energy gap for the $^1D_2$ state is twice as large as that for the other two levels. From that, it would be expected that emission from that level is dominating. However, nonradiative relaxation pathways including multiphonon relaxation and concentration quenching can change this situation, as observed in this case. Under excitation with λ_{ex} = 440 nm ($^3P_J \leftarrow {}^3H_4$), only emission from the $^3P_0$ level was observed. The most intense emission originates from $^3P_0 \rightarrow {}^3H_6$ and $^3P_0 \rightarrow {}^3F_2$ transitions, at ~608 and 643 nm, respectively. The contribution of the greenish-blue luminescence is relatively small, in comparison to the dominant red emission, resulting in an orange emission color of the Pr compound (**2**) (see the color coordinates diagram in Figure 9 (right)).

The Sm compound (**4**) shows a strong orange-red emission. Sm^{3+} has an odd-electron configuration ($4f^5$), implying that the

dx.doi.org/10.1021/ic202655d | Inorg. Chem. 2012, 51, 4679–4688

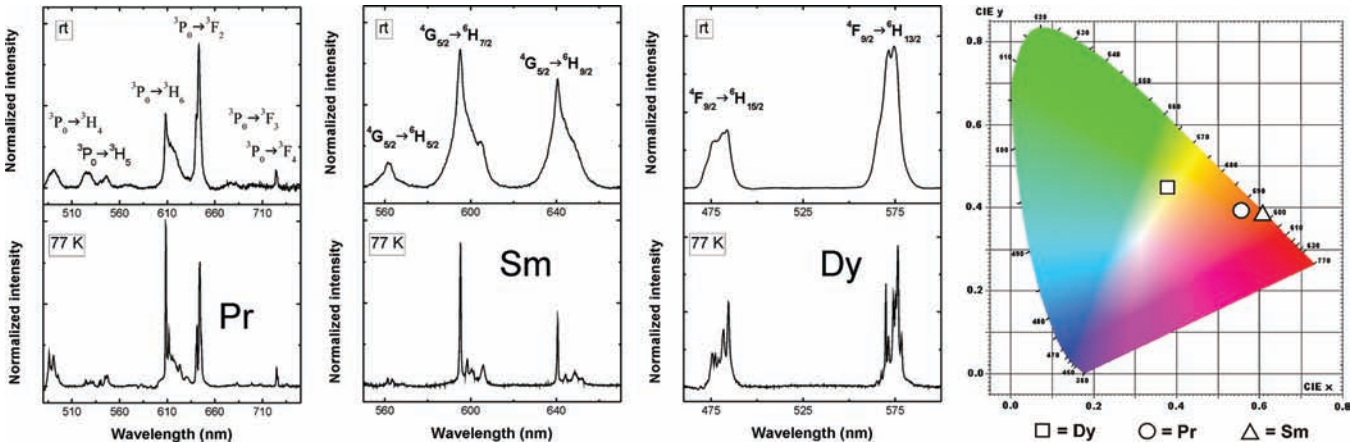

Figure 9. Emission spectra of the $^{2}_{\infty}$[Ln(tfBDC)$(NO_3)$$(DMF)_2$]·DMF compounds (Ln = Pr (**2**), Sm (**4**), Dy (**5**)) at room and at liquid nitrogen temperature (left); color coordinate diagrams of the corresponding emissions (right).

maximum number of Stark components for any symmetry lower than cubic removes the microstate degeneracy, resulting in $J + {}^{1}/_{2}$ Kramer's doublets. The emission spectra both at room temperature and liquid nitrogen temperature consist of three main bands arising from $^4G_{5/2} \rightarrow {}^6H_J$ transitions: the $^4G_{5/2} \rightarrow {}^6H_{5/2}$ transition at 565 nm, the $^4G_{5/2} \rightarrow {}^6H_{5/2}$ transition at 610 nm, and the $^4G_{5/2} \rightarrow {}^6H_{9/2}$ transition at 650 nm. The $^4G_{5/2} \rightarrow {}^6H_{5/2}$ transition at 565 nm has predominantly magnetic dipole character (MD, $\Delta J = 0$), whereas the $^4G_{5/2} \rightarrow {}^6H_{5/2}$ transition at 610 nm is indeed MD allowed, but the electric dipole mechanism (ED) plays the dominant role. The $^4G_{5/2} \rightarrow {}^6H_{9/2}$ transition at 650 nm is of pure ED character. As a result of concentration quenching, the other transitions expected to occur at ∼530 nm were impossible to detect. If Sm^{3+} occupies a low symmetry site, the transitions should be split into the maximum number of Stark components $(J + {}^{1}/_{2})$. Thus, in the emission spectrum of **4**, we should observe three components for the $^4G_{5/2} \rightarrow {}^6H_{5/2}$ transition. In our case, however, the bands remain nonsplit, even at liquid nitrogen temperature. Also, at room temperature, a quite strong broadening of the Sm emission is observed, which points to strong electron−phonon coupling. Among the lanthanide series, Eu^{3+} is well-known as a structural probe. Based on its pure magnetic dipole $^5D_0 \rightarrow {}^7F_1$ transition, which is independent of the chemical environment surrounding the optically active ion, the relative intensity in comparison to the electric dipole transition $^5D_0 \rightarrow {}^7F_2$ is strongly affected by the variation of the ligand field strength and allows studying the site symmetry in detail by luminescence spectroscopy. Such a hypersensitive transition can also be found in Sm^{3+} ($^4G_{5/2} \rightarrow {}^6H_{9/2}$), fulfilling the selection rule $\Delta J = 2$ (electric-dipole allowed). It was proposed to use the $^4G_{5/2} \rightarrow {}^6H_{5/2}$ transition of Sm^{3+} as a reference, because it has a predominant magnetic dipole character ($\Delta J = 0$).[48] The relative intensity of the $^4G_{5/2} \rightarrow {}^6H_{5/2}$ transition, with respect to the $^4G_{5/2} \rightarrow {}^6H_{9/2}$ transition, which is magnetic-dipole forbidden and electric-dipole allowed, supports a low site symmetry for the Sm^{3+} ion in **4**.

The emission spectra of the Dy compound (**5**) are dominated by two strong and sharp transitions, which become even more prominent at low temperatures. The $^4F_{9/2} \rightarrow {}^6H_{13/2}$ transition is located in the yellow range of the spectrum, with the maximum at 575 nm. The second transition ($^4F_{9/2} \rightarrow {}^6H_{13/2}$) is observed at higher energies, with the maximum at 480 nm. The blue emission arises from a magnetic dipole transition, whereas the yellow emission is due to a forced electric dipole. The latter can be considered as a hypersensitive transition based on the selection rules. Since the coordination environment of the optically active ion is able to influence the hypersensitive, electric-dipole-governed transition, while the magnetic dipole transition remains insensitive to the crystal field, a different ratio of the blue to yellow emission can be achieved, thus changing the visible impression of the emission color from blue to white or light yellow. For $^{2}_{\infty}$[Dy(tfBDC)(NO_3)-$(DMF)_2$]·DMF, the emission color was calculated to be in the warm white region of the spectrum, just between white and yellow (see Figure 9, right).

■ CONCLUSION

We have discussed the crystal structures of seven isostructural lanthanide coordination polymers of general composition $^{2}_{\infty}$[Ln-(tfBDC)$(NO_3)$$(DMF)_2$]·DMF ($Ln^{3+}$ = Ce, Pr, Nd, Sm, Dy, Er, Yb), as well as their thermal stability and optical properties. To state that no phase transitions occur at low temperature, investigations of the crystal structure of the Sm compound have been performed exemplarily at 100 K. Although no transition to a low-temperature modification was found, we observed a significant decrease of the interlayer spacing of this two-dimensional framework compound upon cooling. This decrease seems to have a direct effect on the torsion angles of the $tfBDC^{2-}$ linker ligands, which are also reduced at low temperatures. The color of the crystals can be explained by the typical absorption via f−f transitions of the lanthanides in the visible region of light. The Pr, Sm, and Dy compounds show intense bright orange, orange-red, and warm white emissions, respectively. DTA/TG measurements indicate a stepwise loss of DMF solvent molecules upon heating. In future experiments, we plan to investigate the respective intermediates after each loss of DMF molecules. If crystalline samples result, their crystal structures shall be solved and refined from powder diffraction data. A reduction of the DMF content of these compounds should lead to improved luminescence, which shall also be investigated.

A further focus of our work is the syntheses of the remaining lanthanide compounds, especially the congeners containing Eu^{3+}, Tb^{3+}, and Gd^{3+}, from which interesting luminescence properties also are expected.

dx.doi.org/10.1021/ic202655d | Inorg. Chem. 2012, 51, 4679−4688

■ ASSOCIATED CONTENT

Supporting Information

Experimental and simulated powder X-ray diffraction patterns, DTA/TG diagrams, IR spectra and X-ray crystallographic files in CIF format of compounds **1**−**7**. This material is available free of charge via the Internet at http://pubs.acs.org.

■ AUTHOR INFORMATION

Corresponding Author

*Phone: (+49)221-470-3285. Fax: (+49)221-470-3933. E-mail addresses: anja.mudring@rub.de (A.-V.M.), uwe.ruschewitz@uni-koeln.de(U.R.).

Present Address

[#]University of Wrocław, Faculty of Chemistry, Joliot-Curie 14, PL-50383 Wrocław, Poland.

Notes

The authors declare no competing financial interest.

■ ACKNOWLEDGMENTS

We thank Dr. Ingo Pantenburg, Mrs. Ingrid Müller, and Dr. Jörg-Martin Neudörfl for collecting X-ray single crystal data, as well as Mr. Peter Kliesen for DTA/TG and IR measurements and Mrs. Silke Kremer for elemental analysis.

■ DEDICATION

Dedicated to Professor Dieter Naumann on the occasion of his 70th birthday.

■ REFERENCES

(1) Li, H.; Eddaoudi, M.; O'Keeffe, M.; Yaghi, O. M. *Nature* **1999**, *402*, 276−279.

(2) Mueller, U.; Schubert, M.; Teich, F.; Puetter, H.; Schierle-Arndt, K.; Pastré, J. *J. Mater. Chem.* **2006**, *16*, 626−636.

(3) Férey, G. *Chem. Soc. Rev.* **2008**, *37*, 191−214.

(4) Czaja, A. U.; Trukhan, N.; Mueller, U. *Chem. Soc. Rev.* **2009**, *38*, 1284−1293.

(5) Rowsell, J. L. C.; Yaghi, O. M. *Angew. Chem., Int. Ed.* **2005**, *44*, 4670−4679.

(6) Collins, D. J.; Zhou, H.-C. *J. Mater. Chem.* **2007**, *17*, 3154−3160.

(7) Morris, R. E.; Wheatley, P. S. *Angew. Chem., Int. Ed.* **2008**, *47*, 4966−4981.

(8) van den Berg, A. W. C.; Areán, C. O. *Chem. Commun.* **2008**, 668−681.

(9) Eberle, U.; Felderhoff, M.; Schüth, F. *Angew. Chem., Int. Ed.* **2009**, *48*, 6608−6630.

(10) Ma, S.; Zhou, H.-C. *Chem. Commun.* **2010**, *46*, 44−53.

(11) Yang, C.; Wang, X.; Omary, M. A. *J. Am. Chem. Soc.* **2007**, *129*, 15454−15455.

(12) Yang, C.; Wang, X.; Omary, M. A. *Angew. Chem., Int. Ed.* **2009**, *48*, 2500−2505.

(13) Fischer, R. A.; Wöll, C. *Angew. Chem., Int. Ed.* **2008**, *47*, 8164−8168.

(14) Hulvey, Z.; Falcao, E. H. L.; Eckert, J.; Cheetham, A. K. *J. Mater. Chem.* **2009**, *19*, 4307−4309.

(15) Uemura, K.; Maeda, A.; Maji, T. K.; Kanoo, P.; Kita, H. *Eur. J. Inorg. Chem.* **2009**, 2329−2337.

(16) Loiseau, T.; Serre, C.; Huguenard, C.; Fink, G.; Taulelle, F.; Henry, M.; Bataille, T.; Férey, G. *Chem.—Eur. J.* **2004**, *10*, 1373−1382.

(17) Zhang, L.; Wang, Q.; Liu, Y.-C. *J. Phys. Chem. B* **2007**, *111*, 4291−4295.

(18) Hübner, O.; Glöss, A.; Fichtner, M.; Klopper, W. *J. Phys. Chem. A* **2004**, *108*, 3019−3023.

(19) Chen, B.; Yang, Y.; Zapata, F.; Qian, G.; Luo, Y.; Zhang, J.; Lobkovsky, E. B. *Inorg. Chem.* **2006**, *45*, 8882−8886.

(20) Harper, R. J.; Soloski, E. J.; Tamborski, C. *J. Org. Chem.* **1964**, *29*, 2385−2389.

(21) Orthaber, A.; Seidel, C.; Belaj, F.; Pietschnig, R.; Ruschewitz, U. *Inorg. Chem.* **2010**, *49*, 9350−9357.

(22) Seidel, C.; Ahlers, R.; Ruschewitz, U. *Cryst. Growth Des.* **2011**, *11*, 5053−5063.

(23) MacNeill, C. M.; Day, C. S.; Marts, A.; Lachgar, A.; Noftle, R. E. *Inorg. Chim. Acta* **2011**, *365*, 196−203.

(24) Mikhalyova, E. A.; Kolotilov, S. V.; Zeller, M.; Thompson, L. K.; Addison, A. W.; Pavlishchuk, V. V.; Hunter, A. D. *Dalton Trans.* **2011**, *40*, 10989−10996.

(25) Seidel, C.; Ruschewitz, U. *Z. Anorg. Allg. Chem.* **2010**, *636*, 2054.

(26) *Stoe, IPDS Manual*; X-Red 1.22 Stoe Data Reduction Program; Stoe & Cie GmbH: Germany, 2001.

(27) Hooft, R. W. W. *COLLECT*; Nonius BV: Delft, The Netherlands, 1998.

(28) Otwinowski, Z.; Minor, W. In *Methods in Enzymology*, Vol. *276*; Carter, C. W., Jr., Sweet, R. M., Eds.; Macromolecular Crystallography, Part A; Academic Press: New York, 1997; pp 307−326.

(29) Altomare, A.; Cascarano, G.; Giacovazzo, C.; Gualardi, A. *J. Appl. Crystallogr.* **1993**, *26*, 343−350.

(30) (a) Sheldrick, G. M. SHELXL-97: A Program for Crystal Structure Refinement, Release 97-2; University of Göttingen: Göttingen, Germany, 1997. (b) Sheldrick, G. M. *Acta Crystallogr., Sect. A: Found. Crystallogr.* **2008**, *A64*, 112−122.

(31) (a) WinGX-Version 1.64.04, An Integrated System of Windows Programs for the Solution, Refinement and Analysis of Single Crystal X-Ray Diffraction Data; Department of Chemistry, University of Glasgow: Glasgow, U.K., 1997−2002. (b) Farrugia, L. J. *J. Appl. Crystallogr.* **1999**, *32*, 837−838.

(32) Crystallographic data (excluding structure factors) for the structures reported in this paper have been deposited with the Cambridge Crystallographic Data Centre as Supplementary Publication No. CCDC-851205 ($^2_\infty$[Ce(tfBDC)$(NO_3)(DMF)_2$]·DMF (**1**)), CCDC-851209 ($^2_\infty$[Pr(tfBDC)$(NO_3)(DMF)_2$]·DMF (**2**)), CCDC-851208 ($^2_\infty$[Nd(tfBDC)$(NO_3)(DMF)_2$]·DMF (**3**)), CCDC-851211 ($^2_\infty$[Sm(tfBDC)$(NO_3)(DMF)_2$]·DMF at 293 K (**4**)), CCDC-851210 ($^2_\infty$[Sm(tfBDC)$(NO_3)(DMF)_2$]·DMF at 100 K (**4a**)), CCDC-851206 ($^2_\infty$[Dy(tfBDC)$(NO_3)(DMF)_2$]·DMF (**5**)), CCDC-851207 ($^2_\infty$[Er(tfBDC)$(NO_3)(DMF)_2$]·DMF (**6**)), and CCDC-851212 ($^2_\infty$[Yb(tfBDC)$(NO_3)(DMF)_2$]·DMF (**7**)). Copies of the data can be obtained free of charge upon application to CCDC, 12 Union Road, Cambridge CB2 1EZ, U.K. [Fax.: (internat.) + 44 1223/336-033; E-mail: deposit@ccdc.cam.ac.uk].

(33) Win XPow, version 1.04 (07-Jan-1999); Stoe & Cie GmbH: Darmstadt, Germany.

(34) (a) Shannon, R. D.; Prewitt, C. T. *Acta Crystallogr., Sect. B: Struct. Crystallogr. Cryst. Chem.* **1969**, *B25*, 925−946. (b) Shannon, R. D. *Acta Crystallogr., Sect. A: Cryst. Phys. Diffr., Theor. Gen. Crystallogr.* **1976**, *A32*, 751−767.

(35) Hulvey, Z.; Furman, J. D.; Turner, S. A.; Tang, M.; Cheetham, A. K. *Cryst. Growth Des.* **2010**, *10*, 2041−2043.

(36) Wang, Z.; Kravtsov, V. C.; Walsh, R. B.; Zaworotko, M. J. *Cryst. Growth Des.* **2007**, *7*, 1154−1162.

(37) Yen, W. M., Yamamoto, H., Eds. *Phosphor Handbook*, 2nd ed.; CRC Press: Boca Raton, FL, 2007.

(38) Feldmann, C.; Jüstel, T.; Ronda, C. R.; Schmidt, P. J. *Adv. Funct. Mater.* **2003**, *13*, 511−516.

(39) Jüstel, T.; Nikol, H.; Ronda, C. *Angew. Chem., Int. Ed.* **1998**, *37*, 3084−3103.

(40) Höppe, H. A. *Angew. Chem., Int. Ed.* **2009**, *48*, 3572−3582.

(41) Bartolo, B. D.; Chen, X. *Advances in Energy Transfer Processes*; World Scientific: Singapore, 2001.

(42) Binnemans, K.; Görller-Walrand, C. *Chem. Phys. Lett.* **1995**, *235*, 163−174.

(43) Main, J. D. *Nature* **1927**, *120*, 583−584.

(44) Carnall, W. T. In *Handbook on the Physics and Chemistry of Rare Earths,* Vol. 3; Gschneider, K. A., Jr., Eyring, L., Eds.; North−Holland: Amsterdam, 1979; Chapter 24.
(45) Bünzli, J.-C.; Piguet, C. *Chem. Soc. Rev.* **2005**, *34*, 1048−1077.
(46) Auzel, F. *Chem. Rev.* **2004**, *104*, 139−174.
(47) Zhang, Q. Y.; Huang, X. Y. *Prog. Mater. Sci.* **2010**, *55*, 353−427.
(48) Britoa, H. F.; Malta, O. L.; Felinto, M. C.; Teotonio, E. E. S.; Menezes, J. F. S.; Silva, C. F. B.; Tomiyam, C. S.; Carvalho, C. A. A. *J. Alloys Compd.* **2002**, *344*, 293−297.